CHEMISTRY
A EUROPEAN JOURNAL

DOI: 10.1002/chem.200701627

Controllable Synthesis of Nickel Hydroxide and Porous Nickel Oxide Nanostructures with Different Morphologies

Lihong Dong,[a, b] Ying Chu,*[a] and Wendong Sun[a]

Abstract: α-$Ni(OH)_2$ nanobelts, nanowires, short nanowires, and β-$Ni(OH)_2$ nanoplates have been successfully prepared in high yields and purities by a convenient hydrothermal method under mild conditions from very simple systems composed only of NaOH, $NiSO_4$, and water. It has been found that the ratio of NaOH to $NiSO_4$ not only affects the morphology of the $Ni(OH)_2$ nanostructures, but also determines whether the product is of the α- or β-crystal phase. A notable finding is that porous NiO nanobelts were produced after exposure of the $Ni(OH)_2$ products to an electron beam for several minutes during transmission electron microscopy (TEM) observations. Another unusual feature is that rectangular nanoplates with many gaps were obtained. Furthermore, porous NiO nanobelts, nanowires, and nanoplates could also be obtained by annealing the as-prepared $Ni(OH)_2$ products. A sequence of dissolution, recrystallization, and oriented attachment-assisted self-assembly of nanowires into nanobelts is proposed as a plausible mechanistic interpretation for the formation of the observed structures. The method presented here possesses several advantages, including high yields, high purities, low cost, and environmental benignity. It might feasibly be scaled-up for industrial mass production.

Keywords: crystal growth · hydrothermal synthesis · nanostructures · nickel hydroxide · nickel oxide

Introduction

Rechargeable batteries are becoming more and more important in everyday life, especially in consumer electronic devices such as cellular telephones, notebook computers, compact camcorders, and electric vehicles.[1–3] The development of today's electronics industry needs batteries with much higher energy densities. The nickel hydroxide/nickel oxyhydroxide couple $Ni(OH)_2$/NiOOH is the primary redox system used as the positive electrode of alkaline rechargeable batteries, including nickel/cadmium (Ni/Cd), nickel/iron (Ni/Fe), nickel/metal hydride (Ni/MH), and nickel/zinc (Ni/Zn) batteries.[4,5] It has been reported that not only the crystal structure but also the morphology of $Ni(OH)_2$ has a significant influence on its electrochemical properties.[6–8] Han et al.[9] reported that the capacity of the positive electrode could be significantly increased when nanophase $Ni(OH)_2$ was added to micrometer-sized spherical $Ni(OH)_2$. It is anticipated that $Ni(OH)_2$ nanostructures may have potential applications in high-energy-density batteries. They may also be used as precursors for NiO nanostructures, which are well known as valuable materials due to their useful electronic, magnetic, and catalytic properties.[10,11] Such materials have been extensively used in catalysis,[12,17] battery cathodes,[13] gas sensors,[14] electrochromic films,[15] and fuel-cell electrodes.[16] Owing to their fundamental and technological importance, as well as a long history of study, ever more efforts continue to be directed towards exploiting the fabrication of $Ni(OH)_2$ and NiO nanostructures.[18–29] Recently, $Ni(OH)_2$ and NiO hollow or solid micro/nanospheres,[18–23] nanorods,[24] and nanotubes[25] have been reported. By hydrothermal treatment of freshly precipitated nickel oxalate, Wang et al. obtained β-$Ni(OH)_2$ nanoplates.[30] With the assistance of $NH_3{\cdot}H_2O$, $Ni(OH)_2$ nanosheets have been synthesized by a hydrothermal method at 200 °C.[29] Liu's group prepared $Ni(OH)_2$ nanoribbons by hydrothermal treatment of amorphous α-$Ni(OH)_2$ powder in the presence of high concentrations of nickel sulfate.[26,27] Using an ethanol/water/ammonia liquor system, Tang et al. fabricated $Ni(OH)_2$ nanobelts, subsequent annealing of which furnished porous NiO nanobelts.[28] However, in spite of the successes men-

[a] Dr. L. Dong, Prof. Y. Chu, Prof. W. Sun
Department of Chemistry, Northeast Normal University
Changchun, Jilin 130024 (PR China)
Fax: (+86) 431-5684009
E-mail: chuying@nenu.edu.cn

[b] Dr. L. Dong
Department of Chemistry, Tonghua Normal University
Tonghua, Jilin 134002 (PR China)

tioned above, the design of a simpler and more user-friendly protocol for the fabrication of $Ni(OH)_2$ and NiO nanostructures remains a significant challenge. Herein, we report a one-pot, large-scale hydrothermal synthesis of α-$Ni(OH)_2$ nanobelts, nanowires, short nanowires, and β-$Ni(OH)_2$ hexagonal and rectangular nanoplates in a very simple system composed only of water, $NiSO_4$, and NaOH. The effects of the reaction parameters, such as the molar ratio of NaOH to $NiSO_4$ (denoted herein as "*R*"), the temperature, and the reaction time, on morphological and crystallographic phase evolution have been synthetically and systematically investigated. To the best of our knowledge, this is the first systematic study of the factors affecting the crystallographic phase and morphology of $Ni(OH)_2$ nanostructures. The experimental results have confirmed that the hydrothermal method offers a very powerful means of fabricating well crystallized nanostructures, as indicated by our earlier work.[41,42] Furthermore, a notable finding is that porous NiO nanobelts were produced after exposure of the $Ni(OH)_2$ nanobelts to an electron beam for several minutes during transmission electron microscopy (TEM) observations. Moreover, porous NiO nanobelts, nanowires, and nanoplates could also be obtained by annealing the as-prepared $Ni(OH)_2$ products.

Results and Discussion

Figure 1 shows representative scanning electron microscope (SEM) images of $Ni(OH)_2$ nanobelts obtained after hydrothermal reaction for 24 h at 120 °C with $R=3$ (i.e. 9.8 mmol $NiSO_4 \cdot 7H_2O$ and 3.3 mmol NaOH). The images indicate the large quantity and good uniformity of the product; the nanobelts can be seen to have uniform width over their entire lengths. The smooth, thin, belt-like structures have a width typically in the range of 60–80 nm and lengths of up to several tens to several hundreds of micrometers.

Figures 2a and b depict low-magnification TEM images of the nanobelts. The ripple-like contrasts observed in Figure 2b are a result of bending strain, further confirming the characteristic shape of the nanobelts. The thickness of the ribbons ranges between 10 and 20 nm, as estimated from Figure 1b and Figure 2b, and indicated with arrows. The main point to

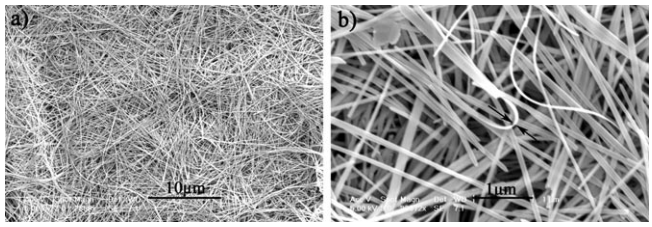

Figure 1. a) Low-magnification and b) high-magnification SEM images of as-obtained $Ni(OH)_2$ nanobelts ($R=3$, 120 °C, 24 h).

emphasize here is that the yield and purity are rather high according to the images. Figure 2c is a higher-magnification TEM image and the inset therein is a lattice-resolved high-resolution transmission electron microscope (HRTEM) image of the part surrounded by the white frame. The HRTEM image clearly reveals (110) atomic planes with a spacing of 0.155 nm, which indicates that the as-synthesized nanobelts are single crystals with a preferential [001] growth direction along their long axes.

An interesting phenomenon was that the as-synthesized nanobelts were very sensitive to electron-beam irradiation under high-vacuum conditions during TEM observation and were transformed into porous structures. As shown in Figures 2d–g, after being irradiated by an electron-beam for several minutes, the sharp lattice fringes of the nanobelts disap-

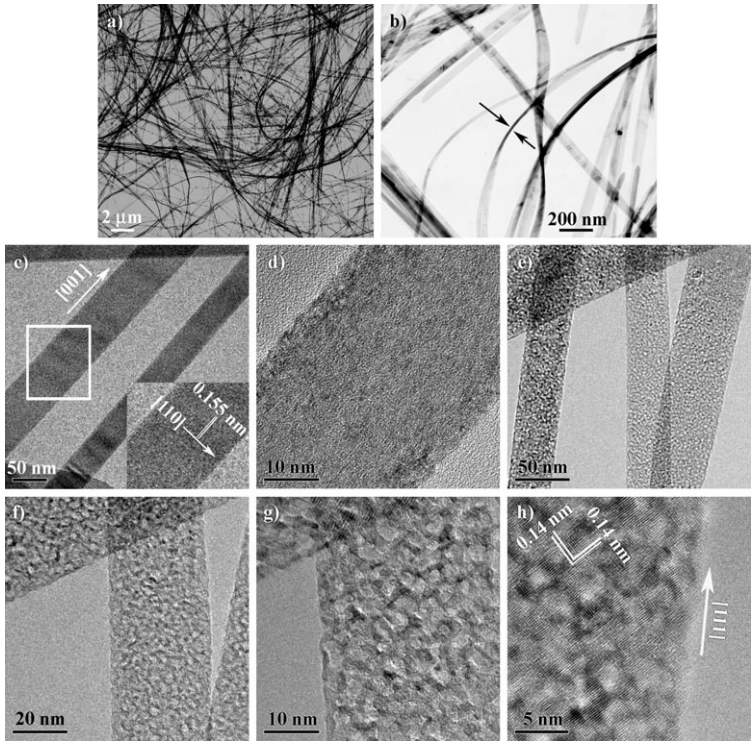

Figure 2. a), b) Low-magnification and c) high-magnification TEM images of as-obtained $Ni(OH)_2$ nanobelts ($R=3$, 120 °C, 24 h); the inset in c) is the HRTEM image of the part surrounded by the white frame. d) A high-magnification TEM image of one $Ni(OH)_2$ nanobelt after irradiation with an electron beam for several minutes. e)–g) Different magnification TEM images of the porous NiO nanobelts obtained by irradiating $Ni(OH)_2$ nanobelts with an electron beam during TEM observation. h) HRTEM image of a porous NiO nanobelt.

peared (Figure 2d) and a copious amount of holes with diameters of several nanometers gradually formed in these nanobelts, while the long belt-like morphology was well maintained. Figures 2e–g are typical TEM images of the porous nanobelts at different magnifications. From Figure 2f and g, it can be seen that most of the holes are square in shape. The HRTEM pattern of a porous nanobelt illustrated in Figure 2h shows a two-dimensional (2D) lattice with a spacing of 0.14 nm, which corresponds to the separation between the (220) planes of cubic NiO (*Fm*3*m*, $a = 4.168$ Å). This indicates that the $Ni(OH)_2$ thermally decomposes to an NiO phase upon electron-beam irradiation under high-vacuum conditions. The HRTEM pattern also reveals that the (111) planes of these NiO nanobelts are parallel to their longitudinal axes, implying that the (111) planes were formerly (001) planes in the original $Ni(OH)_2$ nanobelts. Such smooth conversion of (001) planes in hexagonal $Ni(OH)_2$ to (111) planes in face-centered cubic (fcc) NiO by thermal decomposition is a well-known and well-understood phenomenon for large crystal particles.[24,28,31–34] Therefore, a similar mechanism can be invoked in the case of the present nanobelts.

When the amount of NaOH was increased to 4.9 mmol ($R = 2$) and other conditions were kept the same, nanowires were generated, typical TEM images of which are presented in Figures 3a,b. From Figure 3a, it can be seen that the product was composed of copious amounts of thin, straight, and long nanowires with diameters of 20–30 nm and lengths of several micrometers, these respective dimensions being less than the width and length of the aforementioned nanobelts. An enlarged TEM image of the nanowires is shown in Figure 3b, close inspection of which reveals that each nanowire has a uniform width over its entire length. Again, both images are indicative of high yield and purity. On further increasing the amount of NaOH to 9.8 mmol ($R = 1$), short nanowires were produced; their lengths decreased to 500 nm–1.5 μm, although their diameters were still about 20–30 nm, as shown in Figure 3c. Therefore, it can be concluded that the greater the amount of NaOH used, the shorter the one-dimensional (1D) nanostructures produced. That is to say, NaOH regulates the 1D growth of the nanowires. It follows that 0D nanostructures will be obtained so long as enough NaOH is introduced.

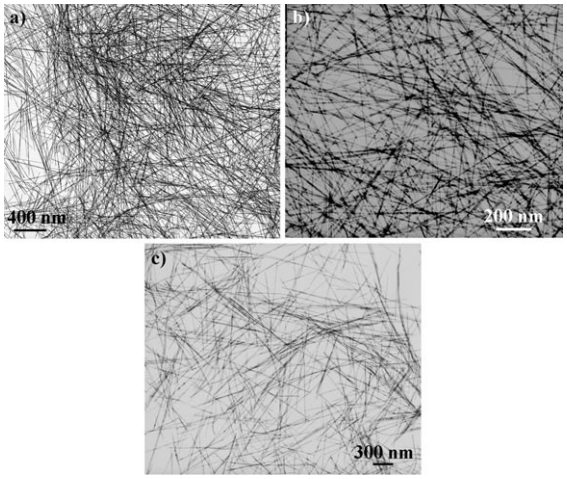

Figure 3. a) Low-magnification and b) high-magnification TEM images of as-obtained $Ni(OH)_2$ nanowires ($R = 2$, 120 °C, 24 h). c) A TEM image of as-obtained $Ni(OH)_2$ short nanowires ($R = 1$, 120 °C, 24 h).

As expected, a further increase in the amount of NaOH to 19.6 mmol ($R = 1/2$) led to the formation of $Ni(OH)_2$ nanoplates, as depicted in Figures 4a and b. It can be seen from the TEM images that most of the nanoplates have a hexagonal morphology with sizes in the range 100–150 nm. Many of them are regular hexagons, with the adjacent edges forming angles of 120°, as indicated by arrows in Figure 4b. As Zhu and co-workers[29] suggested, the surface of the nanoplates is made up of the (0001) planes of the hexagonal β-$Ni(OH)_2$ phase, the angles of 120° may be those of the (10–10) and (01–10) planes, and the edges should correspond to the (10–10) and (01–10) planes. This suggestion is supported by an HRTEM pattern with the [0001] as zone axis, as shown in Figure 4c; clear lattice fringes of 0.27 nm between two adjacent (10–10) and (01–10) planes can be observed. In addition to the nanoplates, some rod-like nanostructures can also be observed in Figure 4a, which presumably arose from a face-to-face stacking of some nanoplates. These stacked structures were further examined by HRTEM, as shown in Figure 4d, which shows a side view of a typical single nanoplate. The calculated interplanar spac-

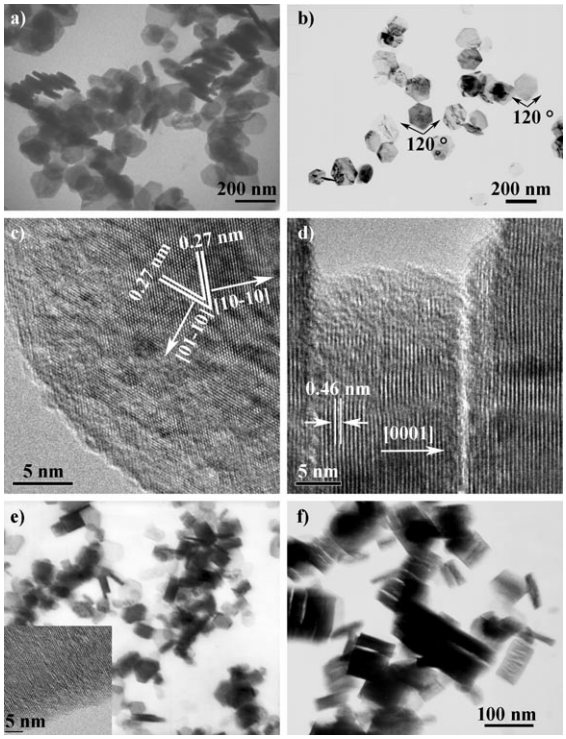

Figure 4. a), b) TEM and c), d) HRTEM images of the as-obtained $Ni(OH)_2$ nanoplates when $R = 1/2$. e) TEM image of the as-obtained $Ni(OH)_2$ nanoplates when $R = 1/3$; the inset is an HRTEM image of a rectangular nanoplate. f) TEM image of the as-obtained $Ni(OH)_2$ nanoplates when $R = 3/40$.

ing is 0.46 nm, which is in good agreement with the *d* spacing value of the (0001) plane of hexagonal β-$Ni(OH)_2$. We also irradiated the nanoplates with an electron beam for a certain time, but no obvious holes appeared on their surfaces. This lack of a phase transformation may be ascribed to stronger binding of water molecules in the nanoplates as compared with that in the nanobelts.

On further decreasing the $[Ni^{2+}]/[OH^-]$ molar ratio to $R=1/3$, a lot of rectangular nanoplates appeared, a typical TEM image of which is shown in Figure 4e. The lengths of these nanoplates were in the range 100–200 nm, while their widths were in the range 50–100 nm. According to the HRTEM image shown as an inset in Figure 4e, the rectangular nanoplates are also single crystals. Moreover, the lower the value of *R*, the more rectangular nanoplates were formed. When *R* was decreased to 3/40, a great number of rectangles with many gaps were formed, as shown in Figure 4f. To the best of our knowledge, this is the first report of this kind of morphology for $Ni(OH)_2$ nanostructures, which should result in an increase in the specific surface area of the product and may open up new possibilities for material applications.

Besides the $[Ni^{2+}]/[OH^-]$ molar ratio, the temperature also had a significant effect on the shape and phase structure of the product when the value of *R* was between 1 and 1/2. In the case of $R=3/4$ and hydrothermal reaction for 24 h, nanoplates were obtained at 120 °C, a typical TEM image of which is shown in Figure 5a. At 140 °C, however, the product was composed of nanobelts and a small amount of nanoplates, as presented in Figure 5b, and an interesting phenomenon was that the nanoplates adhered to the nanobelts and tended to fuse into them. Further increasing the reaction temperature to 160 °C resulted only in the formation of nanobelts, as shown in Figure 5c. When the temperature was further increased to 180 and 200 °C, long and uniform nanobelts remained the only product, as depicted in Figure 5d.

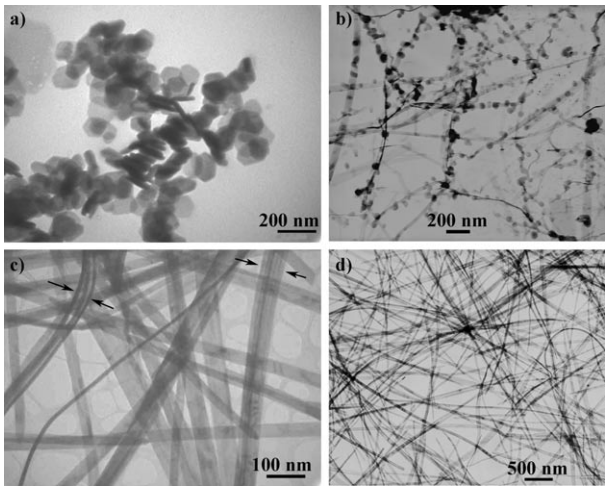

Figure 5. TEM images of the as-obtained $Ni(OH)_2$ nanostructures at different temperatures in the case of $R=3/4$ and hydrothermal reaction for 24 h: a) 120 °C, b) 140 °C, c) 160 °C, d) 180 °C.

To shed light on the mechanism of formation of the $Ni(OH)_2$ nanobelts, their growth process has been followed by examining the products harvested after different hydrothermal treatment times of 0, 0.5, 1, 3, 6, 12, 24, 48, and 96 h at 160 °C, with the value of *R* being fixed at 3. Before hydrothermal treatment, namely at 0 h reaction time, only irregular and flocculated nanoparticles were obtained, as shown in Figure 6a. An XRD pattern (Figure 7a-A) revealed that

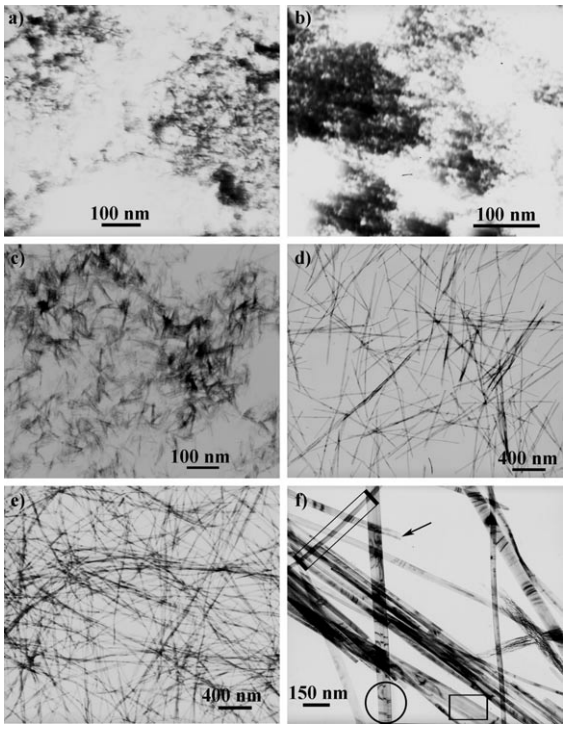

Figure 6. TEM images of the $Ni(OH)_2$ nanostructures harvested after different hydrothermal treatment times at 160 °C with $R=3$: a) 0, b) 0.5, c) 1, d) 3, e) 12, f) 96 h.

they were amorphous, which indicated that hydrothermal treatment was absolutely necessary for the synthesis of $Ni(OH)_2$ nanocrystals. The product obtained after hydrothermal reaction for 0.5 h still consisted of irregular particles, as presented in Figure 6b. When the hydrothermal process was extended to 1 h, a copious amount of short nanofilaments appeared (Figure 6c) and the irregular particles vanished. On prolonging the hydrothermal reaction time to 3 h, the nanofilaments were completely transformed into short nanowires of diameter 20–30 nm and length 1–3 μm, as shown in Figure 6d. After a reaction time of 12 h, the short nanowires grew into longer nanowires with lengths in excess of 10 μm, but their diameter was unchanged from that of the short nanowires obtained after a reaction time of 3 h; a typical TEM image is shown in Figure 6e. When the reaction time was extended to 24, 48, and 96 h, both the length and diameter progressively increased. Figure 6f shows a representative TEM image of the sample after a reaction time of 96 h, close inspection of which reveals several noteworthy features. First, a bifurcation is found at the end of one nano-

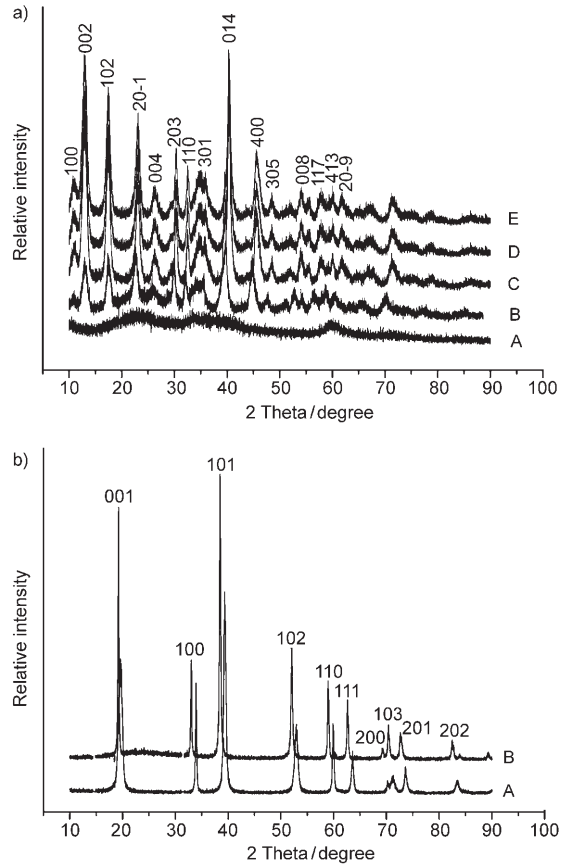

Figure 7. a) XRD patterns of the $Ni(OH)_2$ nanostructures: A) before hydrothermal treatment; B), C), and D) nanobelts, nanowires, and short nanowires obtained by hydrothermal treatment for 24 h at 120 °C with $R=3$, 2, and 1, respectively; E) the mixture of nanobelts and nanoplates obtained by hydrothermal treatment for 24 h at 140 °C with $R=3/4$. b) XRD patterns of A) the hexagonal and B) the rectangular $Ni(OH)_2$ nanoplates.

belt, as indicated by an arrow. Second, parallel fissures are observed in a part of a nanobelt, as marked by the frame; this phenomenon can also be seen in Figure 5c, as indicated by arrows. Third, the ripples on some nanobelts are not consecutive, as highlighted by a circle. On the basis of the above observations, we are inclined to describe the formation process of the $Ni(OH)_2$ nanobelts as involving a sequence of dissolution, recrystallization, and oriented attachment-assisted self-assembly of nanowires into nanobelts, this being a thermodynamically driven process. Under hydrothermal conditions, higher temperature and pressure increased the solubility of fine amorphous α-$Ni(OH)_2$ nanoparticles in water so that a highly supersaturated solution was formed; this was followed by a nucleation and crystallization process of nanocrystals. Due to the difference in solubility between the larger particles and the small particles according to the Gibbs–Thomson law,[38] nanofilaments formed (Figure 6c) as the small particles agglomerated. As the reaction progressed, these nanofilaments extended along their c axes and grew into short and eventually long α-$Ni(OH)_2$ nanowires. Many of these nanowires then aligned in a side-by-side arrangement to form nanowire bundles. Subsequently, these nanowire bundles further crystallized to form single-crystal nanobelts through oriented attachment, which is similar to the formation process of Sb_2O_3 nanobelts reported by Tang's group.[39]

The phase composition and form of the as-synthesized products were examined by X-ray powder diffraction (XRD) analysis. X-ray diffractograms B–D in Figure 7a are those of the as-prepared $Ni(OH)_2$ nanobelts, nanowires, and short nanowires, respectively. All of the diffraction peaks could be clearly indexed to the monoclinic phase α-$Ni(OH)_2$ with lattice constants of $a=7.89$, $b=2.96$, $c=16.63$ Å, and $\beta=91.1°$ in accordance with the standard card JCPDF No. 41–1424. No peaks attributable to other types of nickel hydroxide are observed in the XRD patterns, indicating the high purity of the samples obtained. Diffractogram A in Figure 7a is that of the sample before hydrothermal treatment, which shows it to be amorphous. Diffractogram E in Figure 7a is that of the mixture of nanobelts and nanoplates obtained with $R=3/4$ at a reaction temperature of 140 °C. It can be seen that all of the diffraction peaks in E can be indexed to a monoclinic phase, confirming that the principal morphology of this sample is one of nanobelts, as depicted in Figure 5b. Figure 7b shows the XRD patterns of the hexagonal and rectangular $Ni(OH)_2$ nanoplates, respectively; all of the diffraction peaks are in good agreement with the hexagonal β-$Ni(OH)_2$ structure with lattice constants of $a=3.127$ and $c=4.606$ Å (JCPDS card No. 14-0117). On the basis of the above results, it could be concluded that the crystallographic phase of the as-prepared samples is mainly dependent on the $[Ni^{2+}]/[OH^-]$ molar ratio; that is to say, increasing the amount of NaOH leads to the generation of β-$Ni(OH)_2$.

With a view to obtaining a more comprehensive understanding of the structure transformation and morphology evolution of the $Ni(OH)_2$ nanocrystals, large-scale experiments were carried out under different reaction conditions, and some typical experimental parameters and representative results are listed in Table 1. It can be concluded from the table that the molar ratio of $[OH^-]$ to $[Ni^{2+}]$ was vital in determining the final morphology and crystallographic phase produced. At $R\geq 1$, α-$Ni(OH)_2$ nanobelts or nanowires and short nanowires were always obtained after hydrothermal treatment regardless of the temperature. At $R\leq 1/2$, which is less than the stoichiometry of $Ni(OH)_2$, irrespective of any other conditions, only β-$Ni(OH)_2$ nanoplates were generated, and more and more rectangular nanoplates were formed with increasing amount of NaOH. At $1/2\leq R\leq 1$, such as $R=3/4$, temperature played a very important role in determining the morphology and crystallographic phase of the final product, as discussed above.

Nickel hydroxide ($Ni(OH)_2$) is a typical layered double-hydroxide (LDH), of which there are two polymorphs, namely the α- and β-phases.[35] Both forms crystallize in the hexagonal system with the brucite-type structure by stacking of the $Ni(OH)_2$ layers along the c axis. The main difference between the α- and β-$Ni(OH)_2$ phases arises when other

Table 1. $Ni(OH)_2$ nanobelts/nanowires/short nanowires/nanoplates obtained under different reaction conditions.

$NiSO_4$ [mmol]	NaOH [mmol]	$[Ni^{2+}]/[OH^-]$ (R)	T [°C]	Reaction time [h]	Morphology and shape	Phase
9.8	3.3	3	120	24	nanobelts	α
9.8	4.9	2	120	24	nanowires	α
9.8	4.9	2	120	48	nanobelts	α
9.8	9.8	1	120	24	short nanowires	α
9.8	19.6	1/2	120	24	nanoplates	β
9.8	39.2	1/4	120	24	nanoplates	β
9.8	4.9	2	160	24	nanobelts	α
4.9	3.3	3/2	120	24	short nanowires	α
2.45	3.3	3/4	120	24	nanoplates	β
2.45	3.3	3/4	140	24	nanobelts and nanoplates	α
2.45	3.3	3/4	160	24	nanobelts	α
2.45	3.3	3/4	180	24	nanobelts	α
9.8	3.3	3	80	24	nanobelts	α
1.23	3.3	2/5	180	24	nanoplates	β
9.8	3.3	3	25	0	irregular particles	amorphous
9.8	3.3	3	160	1	short nanofilaments	α
9.8	3.3	3	160	3	short nanowires	α
9.8	3.3	3	160	6	a few short nanobelts	α
9.8	3.3	3	160	12	nanobelts	α
9.8	3.3	3	160	48	nanobelts	α
0.98	3.3	3/30	160	24	nanoplates (rectangles appear)	β
0.49	3.4	3/20	160	24	nanoplates	β
0.25	3.4	3/40	160	24	nanoplates (more rectangles)	β

ions or molecules are present between the stacking layers along the c axis. α-$Ni(OH)_2$ consists of stacked $Ni(OH)_{2-x}$ layers intercalated with various anions[36] (e.g., carbonate, nitrate, sulfate, etc.) or water molecules in the interlayer space to maintain overall charge neutrality.[37] However, β-$Ni(OH)_2$ has a brucite-like ($Mg(OH)_2$) structure without any intercalated species. Nevertheless, the $Ni(OH)_2$ layers of both polymorphs share a common hexagonal planar arrangement of octahedrally oxygen-coordinated Ni^{II} ions. In the present case, when the ratio of Ni^{2+} to OH^- exceeded 1:1, a substantial amount of excess SO_4^{2-} anions was present in the system, and these intercalated into the interlayer spaces of the $Ni(OH)_2$ layers leading to the formation of α-$Ni(OH)_2$. Moreover, due to the stacking of the layers along the c axis, 1D nanowires with [0001] direction were formed. Then, with sufficient energy being provided, the nanowires self-assembled laterally through oriented attachment to minimize the surface energy of the system and further crystallized to form single-crystal nanobelts. When R was decreased to 2, more NaOH was introduced into the reaction system, and this strong electrolyte may have partially neutralized the surface charges of the obtained $Ni(OH)_2$ nanowires, preventing possible crystallite aggregation.[43] The aforementioned oriented attachment of nanowires would then have been prevented so that only nanowires were obtained after reaction for 24 h at 120 °C. Nevertheless, nanobelts could still be obtained by prolonging the reaction time or increasing the temperature in the case of $R=2$, as shown in Table 1, indicating that nanowires could be transformed into nanobelts so long as enough energy was provided. This further confirmed that the nanobelts were formed by a lateral self-assembly of the nanowires. On the other hand, we also noted that when R was varied from 3 to 1, the length of the nanobelts or nanowires decreased with increasing concentration of NaOH and that short nanowires were ultimately formed because NaOH disfavors the anisotropic growth, as pointed out by Liu et al.[40] In addition, NaOH is a strong electrolyte that is selectively adsorbed on certain crystal surfaces; the quantity of hydroxyl functions adsorbed on (0001) faces is much larger than that adsorbed on other faces according to Wang et al.[44] The higher the concentration of NaOH, the greater the steric effect it exerts on the (0001) faces. As a result, the lengths of the one-dimensional nanostructures decreased with increasing concentration of NaOH. Ultimately, when R was less than 1/2, OH^- anions were present in the system in excess, which restricted the intercalation of other species (e.g. SO_4^{2-}) into the as-formed crystal nuclei, and as a result only β-$Ni(OH)_2$ nanoplates were formed. Furthermore, owing to the presence of excess OH^- ions, the strong inhibitory effect on 1D anisotropic growth along the c axis, coupled with the strong steric effect as well as the crystal nature of the hexagonal planar arrangement, led to the formation of hexagonal nanoplates. The precise mechanism of formation of the rectangular nanoplates with gaps still remains a puzzle; more in-depth studies are necessary and the relevant work is underway.

The very interesting phenomenon observed in the case of $R=3/4$, that is, the sole formation of nanoplates at lower reaction temperatures (e.g. 120 °C) and longer and longer 1D nanostructures being synthesized on increasing the temperature to 140, 160, 180, and 200 °C, as shown in Figure 5, can be explained in terms of the relationship between the steric effect exerted by OH^- and the energy provided to overcome this steric effect. At lower temperature, the relatively high OH^- concentration restricted not only the 1D crystal growth but also the intercalation of SO_4^{2-}, and hence β-$Ni(OH)_2$ nanoplates were the exclusive product. When the temperature was increased to 140 °C, the inhibitory effect on the 1D crystal growth was largely overcome and the main product was nanobelts accompanied by a small amount of nanoplates. When the temperature was further increased to 160 °C, a lot of nanobelts were clearly produced, as shown in Figure 5c; some parallel nanowires could also be observed,

but nanoplates were no longer seen owing to the provision of more energy through the higher reaction temperature. As sufficient energy was supplied at the higher reaction temperatures of 180 and 200 °C, the nanobelts became ever more prevalent at the expense of the nanowires. These results further confirmed that temperature can weaken the inhibitory effect of OH^- anions and promote the self-attachment of nanowires into nanobelts.

The thermal behavior of the α-$Ni(OH)_2$ nanobelts and β-$Ni(OH)_2$ nanoplates was investigated by means of TGA and DTA measurements (Figures 8a,b). The TGA curve in Figure 8a indicates that in the temperature range from 30 to 600 °C α-$Ni(OH)_2$ shows two steps at around 65 and 285 °C, with different net weight losses; the total weight loss was measured as about 20 %. The TGA curve of β-$Ni(OH)_2$ (Figure 8b), on the other hand, shows the onset of decomposition (weight loss) at about 285 °C. The major weight loss occurs rapidly between about 298 and 342 °C, as reported in the literature.[29] The total weight loss was measured as about 20 %, in good agreement with the theoretical value (19.4 %) calculated from the following reaction:

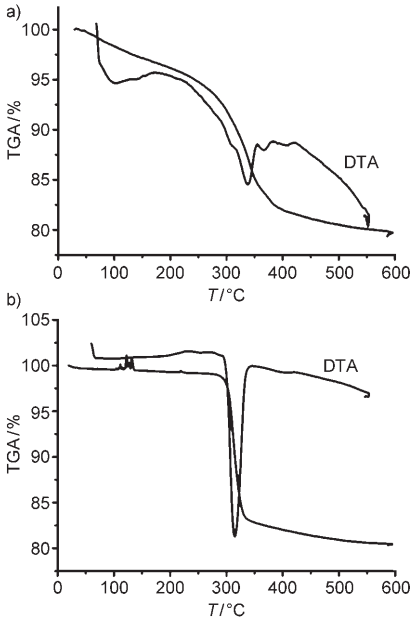

Figure 8. Thermogravimetric curves of a) α-$Ni(OH)_2$ nanobelts and b) β-$Ni(OH)_2$ nanoplates.

$$Ni(OH)_2 \xrightarrow{\text{endothermic}} NiO + H_2O \quad (1)$$

It is believed that the difference in the TGA curves of the two kinds of products may be attributed to the different bonding abilities of water molecules in the respective α- and β-phases, and the TGA results also confirmed the phenomenon that holes appeared on the surfaces of the α-$Ni(OH)_2$ nanobelts but not on the β-$Ni(OH)_2$ nanoplates after irradiation with an electron beam for a certain time during TEM investigation. The DTA curve in Figure 8a shows two endothermic peaks with maxima located at 68 and 345 °C, and the DTA curve in Figure 8b shows one endothermic peak with a maximum located at 318 °C. The temperature ranges of the endothermic peaks in the two DTA curves correspond well to those of the weight losses in the TG curves and are consistent with the endothermic behavior observed during the decomposition of α- and β-$Ni(OH)_2$ into NiO.

Porous NiO nanobelts, nanowires, and nanoplates could be obtained by thermal decomposition of the as-synthesized precursor $Ni(OH)_2$ nanobelts, nanowires, and nanoplates at 500 °C for 2 h. Figures 9a,b show the XRD patterns of NiO nanocrystals obtained from nanobelts and nanoplates as precursors, respectively. The obtained diffractograms reveal that all of the samples could be perfectly indexed to the cubic structure of crystalline NiO and that no impurities were present in the powder samples. The inset in Figure 9 shows low-angle powder X-ray diffraction patterns of the porous NiO nanobelts and nanoplates. The presence of a single broad diffraction peak in the low-angle range is indicative of a disordered mesostructure with no discernible long-range order in the mesopore arrangement.

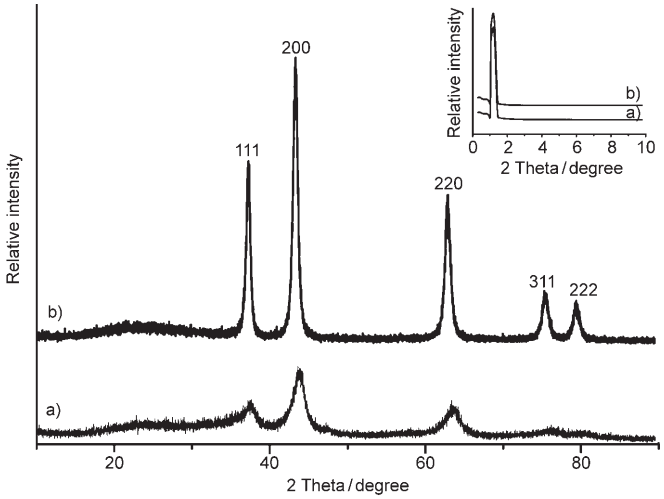

Figure 9. XRD patterns of the porous NiO a) nanobelts and b) nanoplates obtained by thermal decomposition of the as-synthesized $Ni(OH)_2$ nanobelts and nanoplates as precursors at 500 °C for 2 h. The inset shows the corresponding low-angle XRD patterns.

Typical TEM images of the porous NiO nanobelts, nanowires, and nanoplates are shown in Figure 10. It can be seen from Figure 10a that there is an abundance of pores in the nanobelts, and that there is no significant change in the diameter of the nanobelts as compared to their precursors, but that they are much shorter than before calcination, which may stem from the decreased mechanical stability of the porous nanostructures and the sonication to which they were subjected prior to TEM observation. A similar phenomenon was also noted for the porous nanowires, as shown in Figure 10b. Although the morphology of the β-$Ni(OH)_2$ nanoplates, as shown in Figure 10c, was perfectly retained after thermal decomposition to NiO, their size was a little

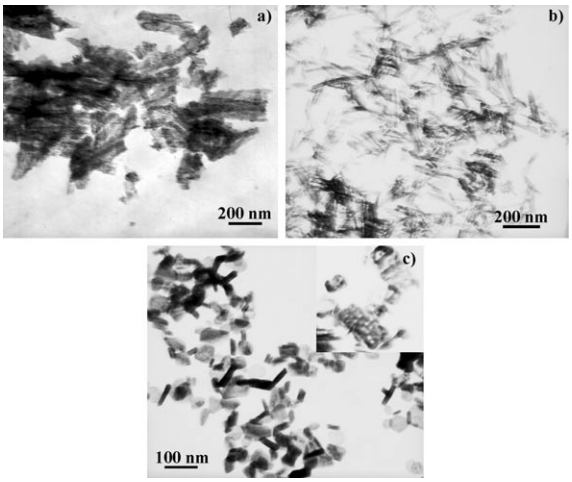

Figure 10. TEM images of the porous NiO structures obtained by thermal decomposition: a) nanobelts, b) nanowires, and c) nanoplates.

smaller than that of the precursors. The inset in Figure 10c is an enlarged image of the porous NiO nanoplates; a lot of holes can clearly be seen, which confirms the porosity of the NiO nanoplates.

To investigate the specific surface areas and porous nature of the NiO nanobelts, nanowires, and nanoplates, Brunauer–Emmett–Teller (BET) gas-sorption measurements were carried out. Nitrogen adsorption–desorption isotherms of these porous nanostructures are shown in Figure 11, and the insets therein are the corresponding Barrett–Joyner–Halenda (BJH) pore size distribution plots. These isotherms can be categorized as being of type IV, with a distinct hysteresis loop. The BET specific surface areas of the samples were found to be 146 $m^2 g^{-1}$ for NiO nanobelts, 147 $m^2 g^{-1}$ for NiO nanowires, and 144 $m^2 g^{-1}$ for NiO nanoplates, indicating that there is no obvious difference in specific surface area among the three kinds of morphology. The average pore diameters according to the BJH plots calculated from the nitrogen isotherms of the porous NiO nanobelts, nanowires, and nanoplates were 11.6, 7.04, and 7.11 nm, respectively, indicating that all of the samples contained mesoscale pores but that the average pore diameters of the NiO nanowires and nanoplates were much smaller than that of the NiO nanobelts. Moreover, the pore size distribution of the NiO nanobelts was seen to be slightly broader according to the BJH pore size distribution plots. Based on the above discussion, it is believed that these porous NiO nanostructures satisfy the requirements for potential applications in the field of surface catalysis and among them the nanowires have the highest specific surface area and the lowest average pore diameter.

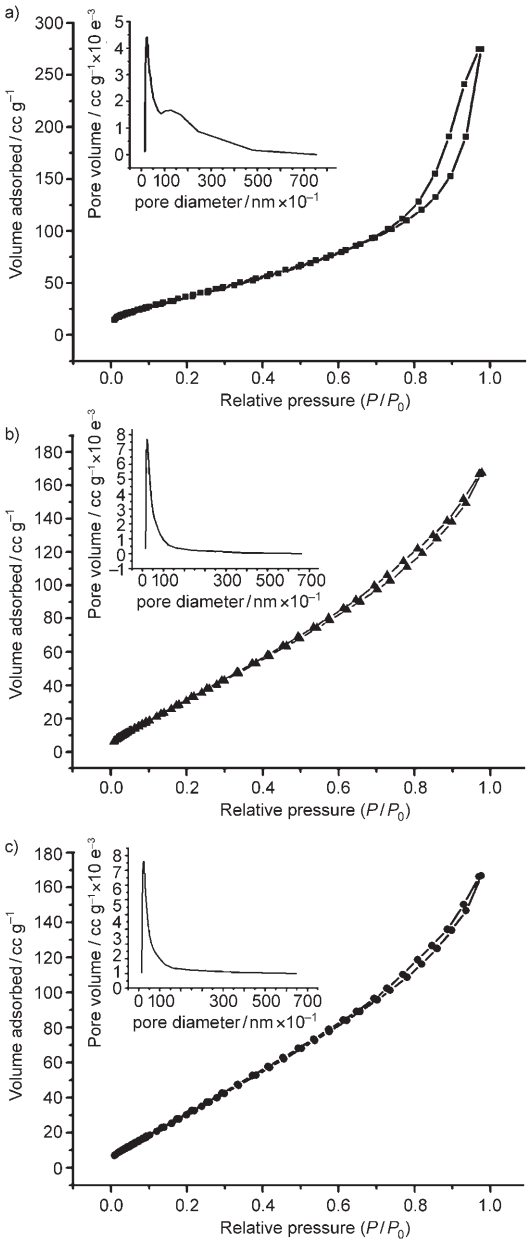

Figure 11. Nitrogen adsorption isotherms of the porous NiO: a) nanobelts, b) nanowires, and c) nanoplates. The insets show the corresponding Barrett–Joyner–Halenda (BJH) pore size distribution plots.

Conclusion

In summary, by hydrothermal treatment of a very simple system composed only of water, $NiSO_4$, and NaOH, and modulating the ratio of NaOH to $NiSO_4$, some $Ni(OH)_2$ nanostructures of various morphologies have been obtained. Thus, α-phase nanobelts, nanowires, and short nanowires, and β-phase hexagonal and rectangular nanoplates could be synthesized exclusively, in high yields and with high purities. By irradiation with an electron beam for several minutes, the as-synthesized nanobelts were transformed into porous NiO nanobelts, but the nanoplates underwent no obvious changes under the same conditions. All of the as-prepared $Ni(OH)_2$ products could be transformed into corresponding porous NiO nanostructures by annealing. The formation process of the $Ni(OH)_2$ nanostructures may be described as a sequence of dissolution, recrystallization, and oriented at-

tachment-assisted self-assembly of nanowires into nanobelts. The current process has the advantages of employing simple synthetic methods and inexpensive experimental set-ups that may readily be scaled-up for industrial production.

Experimental Section

Preparation of samples: All of the chemicals were of analytical grade and were used without further purification. Distilled water was used throughout. In a typical preparation of α-$Ni(OH)_2$ nanobelts, an aqueous solution (40 mL) containing $NiSO_4 \cdot 7H_2O$ (9.8 mmol) and NaOH (3.3 mmol) was sealed into a 50 mL capacity Teflon-lined autoclave and heated at 120 °C for 24 h (the reaction time was always 24 h unless otherwise mentioned). After hydrothermal treatment, the reaction mixture separated into a green paste-like precipitate and a clear supernatant, which was decanted off. The solid product was subsequently washed several times with deionized water, and then dried in air at 60 °C for 12 h. Finally, a green powder was obtained. By changing the molar ratio of $NiSO_4$ to NaOH, the temperature, or the reaction time, α-$Ni(OH)_2$ nanowires, short nanowires, and β-$Ni(OH)_2$ nanoplates could be obtained. Porous NiO nanobelts, nanowires, and nanoplates were obtained when the as-synthesized $Ni(OH)_2$ nanobelts, nanowires, and nanoplates were directly calcined at 500 °C for 2 h in a muffle furnace.

Characterization: The as-prepared powder samples were characterized by X-ray powder diffraction (XRD) analysis on a Rigaku X-ray diffractometer with $Cu_{K\alpha}$ radiation ($\lambda = 1.5406$ Å). The morphologies and sizes of the as-obtained products were observed by transmission electron microscopy (TEM, Hitachi H-800) and field-emission scanning electron microscopy (FE-SEM, JEOL 7500 B). High-resolution transmission electron microscopy (HRTEM) was performed with a JEM-3010 transmission electron microscope (300 kV). Thermogravimetric (TG) analyses were carried out with an STA-409 PC/4/H Luxx simultaneous TG-DTA/DSC apparatus (Germany) at a heating rate of 10 °C min^{-1} in a flow of air. N_2 adsorption was determined by BET measurements using an ASAP-2000 surface area analyzer.

Acknowledgement

This work was supported by the Natural Science Fund of China (No. 20573017) and the Analysis and Testing Foundation of Northeast Normal University.

[1] S. R. Ovshinsky, M. A. Fetcenko, J. Ross, *Science* **1993**, *260*, 176.
[2] M. S. Dresselhaus, I. L. Thomas, *Nature* **2001**, *414*, 332.
[3] J. M. Tarascon, M. Armand, *Nature* **2001**, *414*, 359.
[4] J. McBreen, in *Modern Aspects of Electrochemistry*, Vol. 21 (Eds.: R. E. White, J. O'M. Bockris, B. E. Conway), Plenum, New York, **1990**, p. 29.
[5] D. Linden, *Handbook of Batteries*, 3rd ed., McGraw-Hill, New York, **2002**.
[6] M. C. Bernard, R. Cortes, M. Keddam, H. Takenouti, P. Bernard, S. Senyarich, *J. Power Sources* **1996**, *63*, 247.
[7] K. Watanabe, T. Kikuoka, *J. Appl. Electrochem.* **1995**, *25*, 219.
[8] D. E. Reisner, A. J. Salkind, P. R. Strutt, T. D. Xiao, *J. Power Sources* **1997**, *65*, 231.
[9] X. J. Han, X. M. Xie, C. Q. Xu, D. R. Zhou, Y. L. Ma, *Opt. Mater.* **2003**, *23*, 465.
[10] M. Rubinsteina, R. H. Kodamab, S. A. Makhlouf, *J. Magn. Magn. Mater.* **2001**, *234*, 289.
[11] V. Biju, M. A. Khadar, *Mater. Res. Bull.* **2001**, *36*, 21.
[12] R. M. Tost, J. S. González, P. M. Torres, E. R. Castellón, A. J. López, *J. Mater. Chem.* **2002**, *12*, 3331.
[13] B. Huang, Q. C. Yu, H. M. Wang, G. Chen, K. A. Hu, *J. Power Sources* **2004**, *137*, 163.
[14] I. Hotovy, V. Rehacek, P. Siciliano, S. Capone, L. Spiess, *Thin Solid Films* **2002**, *418*, 9.
[15] E. L. Mille, R. E. Rocheleau, *J. Electrochem. Soc.* **1997**, *144*, 3072.
[16] R. C. Makkus, K. Hemmes, J. H. Dewit, *J. Electrochem. Soc.* **1994**, *141*, 3429.
[17] Z. Xu, Y. M. Li, J. Y. Zhang, L. Chang, R. Q. Zhou, Z. T. Duan, *Appl. Catal. A* **2001**, *213*, 65.
[18] Y. Wang, Q. S. Zhu, H. G. Zhang, *Chem. Commun.* **2005**, 5231.
[19] D. B. Wang, C. X. Song, Z. S. Hu, X. Fu, *J. Phys. Chem. B* **2005**, *109*, 1125.
[20] B. H. Liu, S. H. Yu, S. F. Chen, C. Y. Wu, *J. Phys. Chem. B* **2006**, *110*, 4039.
[21] J. Q. Qi, T. Zhang, M. Lu, Y. Wang, W. P. Chen, L. T. Li, H. L. W. Chan, *Chem. Lett.* **2005**, *34*, 180.
[22] M. H. Cao, X. Y. He, J. Chen, C. W. Hu, *Cryst. Growth Des.* **2007**, *7*, 170.
[23] J. Liu, S. F. Du, L. Q. Wei, H. D. Liu, Y. J. Tian, Y. F. Chen, *Mater. Lett.* **2006**, *60*, 3601.
[24] K. Matsui, T. Kyotani, A. Tomita, *Adv. Mater.* **2002**, *14*, 1216.
[25] F. S. Cai, G. Y. Zhang, J. Chen, X. L. Gou, H. K. Liu, S. X. Dou, *Angew. Chem.* **2004**, *116*, 4308; *Angew. Chem. Int. Ed.* **2004**, *43*, 4212.
[26] D. N. Yang, R. M. Wang, J. Zhang, Z. F. Liu, *J. Phys. Chem. B* **2004**, *108*, 7531.
[27] D. N. Yang, R. M. Wang, M. S. He, J. Zhang, Z. F. Liu, *J. Phys. Chem. B* **2005**, *109*, 7654.
[28] Y. W. Tang, Z. Y. Jia, Y. Jiang, L. Y. Li, J. B. Wang, *Nanotechnology* **2006**, *17*, 5686.
[29] Z. H. Liang, Y. J. Zhu, X. L. Hu, *J. Phys. Chem. B* **2004**, *108*, 3488.
[30] X. Wang, L. Li, Y. G. Zhang, Sh. T. Wang, Z. D. Zhang, L. F. Fei, Y. T. Qian, *Cryst. Growth Des.* **2006**, *6*, 2163.
[31] L. X. Yang, Y. J. Zhu, H. Tong, Z. H. Liang, W. W. Wang, *Cryst. Growth Des.* **2007**, *7*, 2716.
[32] L. Durand-Keklikian, I. Haq, E. Matijevic, *Colloids Surf.* **1994**, *92*, 267.
[33] C. L. Cronan, F. J. Micale, M. Topic, H. Leidheiser, A. C. Zettlemoyer, *J. Colloid Interface Sci.* **1976**, *55*, 546.
[34] C. J. C. Carpenter, Z. S. Wronski, *Nanostruct. Mater.* **1999**, *11*, 67.
[35] P. Oliva, J. Leonardi, J. F. Laurent, C. Delmas, J. J. Braconnier, M. Figlarz, F. Fievet, *J. Power Sources* **1982**, *8*, 229.
[36] M. Kurmoo, P. Day, A. Derory, C. Estournes, R. Poinsot, M. J. Stead, C. J. Kepert, *J. Solid State Chem.* **1999**, *145*, 452.
[37] a) F. Portemer, A. Delahyde-Vidal, M. Figlarz, *J. Electrochem. Soc.* **1992**, *139*, 671; b) A. Delahyde-Vidal, K. Tekaia-Ehlsissen, P. Genin, M. Figlarz, *J. Solid State Inorg. Chem.* **1994**, *31*, 823; c) P. V. Kamath, G. H. A. Therese, J. Gopalakrishnan, *J. Solid State Inorg. Chem.* **1997**, *128*, 38.
[38] J. W. Mullin, *Crystallization*, Butterworth-Heinemann, Woburn, MA, **1997**.
[39] Z. T. Deng, D. Chen, F. Q. Tang, X. W. Meng, J. Ren, L. Zhang, *J. Phys. Chem. C* **2007**, *111*, 5325.
[40] J. P. Liu, X. T. Huang, Y. Y. Li, K. M. Sulieman, X. He, F. L. Sun, *J. Mater. Chem.* **2006**, *16*, 4427.
[41] Y. Liu, Y. Chu, L. L. Li, L. H. Dong, Y. J. Zhuo, *Chem. Eur. J.* **2007**, *13*, 7926.
[42] Y. Liu, Y. Chu, Y. J. Zhuo, L. H. Dong, L. L. Li, M. Y. Li, *Adv. Funct. Mater.* **2007**, *17*, 933.
[43] W. L. Fan, X. Y. Song, Y. X. Bu, S. X. Sun, X. Zhao, *J. Phys. Chem. B* **2006**, *110*, 23247.
[44] H. L. Xu, W. Z. Wang, W. Zhu, *Mater. Lett.* **2006**, *60*, 2203.

Received: October 15, 2007
Revised: January 21, 2008
Published online: April 9, 2008

